JOURNAL OF MECHANICS OF CONTINUA AND MATHEMATICAL SCIENCES
www.journalimcms.org

ISSN (Online) : 2454 -7190 , Special Issue, No.-12, August (2025) pp 94-111 ISSN (Print) 0973-8975

ANALYTICAL MODELING OF SINTER FORGING AT HIGH SPEED CONSIDERING VARIOUS FRICTION CONDITIONS

Navdeep[1], Parveen Kumar[2], R. K. Ranjan[3], K. D. Sharma[4]

[1,2] Department of Mathematics, J. C. Bose University of Science and Technology, Sector-6, Faridabad, Haryana, 121006, India.

[3] Department of Mechanical Engineering, Government Polytechnic, Vidya Peeth Chowk, Lakhisarai, Bihar, 811311, India.

[4] Department of Mathematics, Chitkara University Institute of Engineering and Technology, Punjab, 140401, India.

Corresponding author: **Parveen Kumar**

Email: [1]navdeepvar394@gmail.com, [2] parveengaur1980@gmail.com
[3] rkranjanbit@gmail.com, [4] krishandutt.sharma@chitkara.edu.in

https://doi.org/10.26782/jmcms.spl.12/2025.08.00008

(Received: May 16, 2025; Revised: July 26, 2025; Accepted: August 09, 2025)

Abstract

This study investigates the influence of die velocity in sinter forging, particularly focusing on plastic deformation characteristics in the cold forging of axially symmetric components. Key factors such as material flow, inertia energy dissipation, and die load are examined. Results show that both energy dissipation and die load increase with higher die speeds. Utilizing an upper-bound approach with a simplified velocity field, theoretical results for the average die load are established. This analysis aims to improve the understanding of dynamic effects in sinter-forging cylindrical preforms, offering valuable insights for future research in this domain.

Additionally, this paper provides a comprehensive review of the role of friction in metal forming processes, emphasizing the development of theoretical models to analyze tool-workpiece interfaces under varying friction conditions using the upper-bound method. The importance of understanding friction, particularly in forging processes, is highlighted. A composite friction mechanism in axisymmetric forging is introduced, accounting for the effect of platen speed. The significance of friction conditions on key factors such as applied load and plastic deformation is underscored, particularly considering the crucial interaction between adhesion and sliding.

Keywords: Sinter forging, Upper bound, Die Load, Dynamical effect, sticking and sliding friction

I. Introduction

I.i. Introduction to Sinter Forging

Sinter forging has emerged as a rapidly advancing net-shape manufacturing technique, offering the ability to mass-produce high-performance, precise engineering components at competitive rates while minimizing material waste. This hybrid process merges the strengths of powder metallurgy and conventional forging, creating a robust metallurgical structure through powder metallurgy and imparting desirable mechanical properties through the forging process. The combination of these two methods results in final products with mechanical and metallurgical properties comparable to wrought materials, thus enhancing product quality and performance. Additionally, sinter forging helps reduce energy consumption by eliminating energy-intensive operations, making it an attractive alternative for industries seeking to improve efficiency and sustainability in metal forming processes [IX]. Recent years have witnessed a significant surge in the use of sintered metal products, attributed to their ease of manufacturability and the superior surface finish of the final product. This has led to substantial cost reductions in secondary finishing processes such as grinding and buffing [III, XV].

I.ii. Research Interest and Motivation

Sinter forging has been a subject of extensive research over the past 50 years, driven by the need to enhance its application at the industrial level for metal forming. Researchers are particularly focused on optimizing the process to reduce energy consumption and minimize scrap production, all while improving resource efficiency.

The applied pressure during the forging process depends significantly on the frictional conditions, with or without adhesion, and has been the focus of extensive research. When adhesion is considered, the interaction between the tool and workpiece involves both sliding and adhesive forces, which contribute to higher friction levels and thus, higher applied pressure. Both assumptions of friction with adhesion and friction without adhesion have profound implications for product quality and process efficiency, influencing factors such as die load, metal flow in the final product [VI, XX]. For instance, the coefficient of friction plays a crucial role in determining the applied load, with friction increasing in the absence of lubrication [XXI]. Unlike conventional forging, where wrought metals are formed, sinter forging involves additional complexities due to the porous nature of the preforms. The presence of porosity alters the deformation behavior, making it necessary to consider mass constancy rather than volume constancy during compression.

I.iii. Deformation Characteristics and Forging Speed

The deformation characteristics of sintered metal during forging differ significantly from those of wrought materials due to the porosity present in the sintered preform. This porous nature affects the flow stress, which varies with the speed of forging. At high speeds, the flow stress of sintered metals behaves differently than at low speeds, requiring careful consideration during the process design [1, 7]. The influence of forging speed on deformation behavior is one of the key factors impacting the final product quality in sinter forging [X, XVII].

I.iv. Modeling and Analysis

Few researchers have devoted efforts to developing comprehensive mathematical models to analyze the dynamic effects in sinter forging [X, XI, XII]. The behavior of sintered metals during the forging process is complex due to factors like porosity, friction, and relative density, making mathematical modeling crucial for understanding and predicting outcomes. Various modeling methods, such as equilibrium analysis, upper bound, and lower bound techniques, have been used to simulate and quantify these parameters. These models contribute significantly to understanding how friction, forging speed, and plastic deformation affect the sinter forging process, offering valuable insights into improving efficiency and performance in industrial applications.

I.v. Complexity of Process Parameters

The relationship between process parameters in sinter forging, such as forging speed, pressure, and friction, is highly complex. Ongoing research aims to deepen the understanding of how these parameters interact and influence each other, to improve the efficiency and quality of the sinter forging process. Researchers continue to investigate these dependencies, striving to optimize the process for diverse industrial applications.

I.vi. Contributions of the Paper

The contributions presented in this paper offer a comprehensive overview of the crucial role played by different types of friction in metal forming processes, particularly over the last five decades. Our work includes a review of theoretical models, with an emphasis on the impact of friction at the tool-workpiece interface in forging processes. Notably, friction in sinter forging depends heavily on the kind of friction, and efforts to quantify this coefficient have provided critical insights into determining the applied load during forging [V, VII]. Additionally, this paper builds upon traditional theories, such as constant shear factors, Coulomb friction, and viscous friction, to investigate the interaction between the die and preform during plastic deformation. Moreover, high friction due to direct metal-to-metal contact can deteriorate the product, which is why the use of lubricants is essential in sinter forging [I, VIII].

I.vii. Frictional Considerations in Sinter Forging

This paper introduces a composite friction mechanism, prevalent in axisymmetric forging, that incorporates Rook's law of friction while accounting for the effects of platen speed [X, XI, XVIII]. The conditions of friction between the deforming tool and the workpiece are critical for determining factors such as applied load, plastic deformation, and surface finish. The interaction between adhesion and sliding friction is especially crucial in this context. In metal forming, particularly in the forging of metal-powder preforms, the metal flow pattern reveals two distinct zones: the sticking zone and the sliding zone. The sticking zone, characterized by the absence of relative movement between the workpiece and the die, plays an important role in shaping the deformation behavior. Meanwhile, the sliding zone adds further complexity to the process dynamics. Understanding these dual zones is vital for optimizing the sinter forging process and ensuring high-quality outcomes.

In conclusion, this paper highlights the significance of friction in sintered metal forming, especially in terms of its effect on die loads, metal flow, and the overall quality of the finished product. Through analytical modeling and experimental validation, our findings underscore the potential for sinter forging to be effectively applied across diverse industrial scenarios. The promising results demonstrated in this work point towards future advancements in optimizing sinter forging for large-scale production.

II. Analytical Modeling

The use of analytical models in sinter forging reduces costs and offers a methodical way to shape the finished result. Through the quantification of the effects of various parameters, process optimisation is made possible, leading to increased efficiency and lower costs. Moreover, analytical models serve as a valuable tool for identifying areas for further investigation. By highlighting critical factors and their interactions, they guide researchers towards exploring new avenues and refining existing methodologies.

The analytical model proposed herein offers a quantifiable framework for assessing a range of processing parameters in sinter forging. By breaking down the process into energy dissipation components and analyzing their behavior mathematically, this model enables a deeper understanding of the process dynamics. Energy component and frictional condition equations are taken as Appendix A, Appendix B, respectively, during the plastic deformation in sinter forging.

Internal Energy Dissipation

$$W_i = \frac{2\lambda}{\sqrt{3}} \int_0^h \int_0^b \sqrt{\frac{1}{2}\left(\dot{\varepsilon}_{rr}^2 + \dot{\varepsilon}_{\theta\theta}^2 + \dot{\varepsilon}_{zz}^2\right)}.2\pi r dr dz$$

$$W_i = \sqrt{\frac{2}{3}}\pi\lambda U b^2 \sqrt{1 + \frac{1}{2}\left(\frac{1-2\eta}{1+\eta}\right)^2}$$

Shear Frictional Energy Dissipation

$W_f = \int_0^b \tau(|U_r|_{z=0} + |U_r|_{z=h}).2\pi r dr$; in case of sliding friction only

$W_{\mathrm{f}} = \frac{2\pi U(1-2\eta)\mu p_{av} b^3}{(1+\eta)h} \times \frac{1}{3}$ in the case of sliding and sticking friction

$$W_{\mathrm{f}} = \frac{2\pi U(1-2\eta)\mu p_{av} b^3}{(1+\eta)h}\left[\frac{1}{3} + x\left\{\frac{1}{3}\left(1 - \frac{1}{4n}\right)\right\}\right]$$

in the case of sliding and sticking friction with the sticking zone.

$$W_{\mathrm{f}} = \frac{2\pi U(1-2\eta)\mu p_{av} b^3}{(1+\eta)h}\left[\frac{1}{3} + x\left\{\frac{1}{3}\left(1 - \frac{r_m}{nb}\right) + \frac{1}{4n}\right\}\right]$$

for practicality, consider $p = p_{av}$, where $p_{av} = \frac{P}{\pi b^2}$ Shear frictional energy also has linear proportionality with speed.

Inertial Energy Dissipation

$$W_{\mathrm{a}} = \int_0^b \int_0^h \rho_{\mathrm{p}}(a_r U_r + a_z U_z) 2\pi r \, \mathrm{d}r \, \mathrm{d}z$$

where $a_r = \left(\frac{(1-2\eta)}{2(1+\eta)}\frac{r}{h}\right)\left[\frac{(1-2\eta)}{2(1+\eta)}\frac{U^2}{h} + \dot{U}\right] a_z = \frac{z}{h}\left(\frac{U^2}{h} - \dot{U}\right)$

$$W_a = \pi\rho_p U b^2 \left[\left(\frac{(1-2\eta)U^2}{2(1+\eta)h} + \dot{U}\right)\left(\frac{1-2\eta}{2(1+\eta)}\right)\frac{b^2}{2} - \frac{U^2 - \dot{U}h}{3}\right]$$

III. Forging load, P

P, die load when considering only sliding friction

$$P = \frac{\sqrt{\frac{2}{3}}\pi\lambda b^2\sqrt{1+\frac{1}{2}\left(\frac{1-2\eta}{1+\eta}\right)^2} + \pi\rho_p b^2\left[\left(\frac{(1-2\eta)U^2}{2(1+\eta)h} + \dot{U}\right)\left(\frac{1-2\eta}{2(1+\eta)}\right)\frac{b^2}{2} - \frac{U^2-\dot{U}h}{3}\right]}{1 - \frac{2(1-2\eta)\mu b}{(1+\eta)h}\left(\frac{1}{3}\right)}$$

P, die load when considering sliding and sticking friction without a sticking zone

$$P = \frac{\sqrt{\frac{2}{3}}\pi\lambda b^2\sqrt{1+\frac{1}{2}\left(\frac{1-2\eta}{1+\eta}\right)^2} + \pi\rho_p b^2\left[\left(\frac{(1-2\eta)U^2}{2(1+\eta)h} + \dot{U}\right)\left(\frac{1-2\eta}{2(1+\eta)}\right)\frac{b^2}{2} - \frac{U^2-\dot{U}h}{3}\right]}{1 - \frac{2(1-2\eta)\mu b}{(1+\eta)h}\left(\frac{1}{3} + x\left\{\frac{1}{3} - \frac{1}{4n}\right\}\right)}$$

P, die load when considering sliding and sticking friction with the sticking zone

$$P = \frac{\sqrt{\frac{2}{3}}\pi\lambda b^2\sqrt{1+\frac{1}{2}\left(\frac{1-2\eta}{1+\eta}\right)^2} + \pi\rho_p b^2\left[\left(\frac{(1-2\eta)U^2}{2(1+\eta)h} + \dot{U}\right)\left(\frac{1-2\eta}{2(1+\eta)}\right)\frac{b^2}{2} - \frac{U^2-\dot{U}h}{3}\right]}{1 - \frac{2(1-2\eta)\mu b}{(1+\eta)h}\left(\frac{1}{3} + x\left\{\frac{1}{3}\left(1 - \frac{r_m}{nb}\right) + \frac{1}{4n}\right\}\right)}$$

p_{av}, average pressure when considering only sliding friction

$$p_{av} = \frac{\sqrt{\frac{2}{3}}\lambda\sqrt{1+\frac{1}{2}\left(\frac{1-2\eta}{1+\eta}\right)^2} + \rho_p\left[\left(\frac{(1-2\eta)U^2}{2(1+\eta)h} + \dot{U}\right)\left(\frac{1-2\eta}{2(1+\eta)}\right)\frac{b^2}{2} - \frac{U^2-\dot{U}h}{3}\right]}{1 - \frac{2(1-2\eta)\mu b}{(1+\eta)h}\left(\frac{1}{3}\right)}$$

p_{av}, average pressure when considering only sliding and sticking friction without the sticking zone.

$$p_{av} = \frac{\sqrt{\frac{2}{3}}\lambda\sqrt{1+\frac{1}{2}\left(\frac{1-2\eta}{1+\eta}\right)^2} + \rho_p\left[\left(\frac{(1-2\eta)U^2}{2(1+\eta)h} + \dot{U}\right)\left(\frac{1-2\eta}{2(1+\eta)}\right)\frac{b^2}{2} - \frac{U^2-\dot{U}h}{3}\right]}{1 - \frac{2(1-2\eta)\mu b}{(1+\eta)h}\left(\frac{1}{3} + x\left\{\frac{1}{3} - \frac{1}{4n}\right\}\right)}$$

p_{av}, average pressure when considering sliding and sticking friction with the sticking zone

$$p_{av} = \frac{\sqrt{\frac{2}{3}}\lambda\sqrt{1+\frac{1}{2}\left(\frac{1-2\eta}{1+\eta}\right)^2} + \rho_p\left[\left(\frac{(1-2\eta)U^2}{2(1+\eta)h}+\dot{U}\right)\left(\frac{1-2\eta}{2(1+\eta)}\right)\frac{b^2}{2} - \frac{U^2-\dot{U}h}{3}\right]}{1-\frac{2(1-2\eta)\mu b}{(1+\eta)h}\left(\frac{1}{3}+x\left\{\frac{1}{3}\left(1-\frac{r_m}{nb}\right)+\frac{1}{4n}\right\}\right)}$$

$$\frac{p_{av}}{\lambda} = \frac{\sqrt{\frac{2}{3}}\sqrt{1+\frac{1}{2}\left(\frac{1-2\eta}{1+\eta}\right)^2} + \frac{\rho_p}{\lambda}\left[\left(\frac{(1-2\eta)U^2}{2(1+\eta)h}+\dot{U}\right)\left(\frac{1-2\eta}{2(1+\eta)}\right)\frac{b^2}{2} - \frac{U^2-\dot{U}h}{3}\right]}{1-\frac{2(1-2\eta)\mu b}{(1+\eta)h}\left(\frac{1}{3}+x\left\{\frac{1}{3}\left(1-\frac{r_m}{nb}\right)+\frac{1}{4n}\right\}\right)}$$

Inertial Factor

$$\zeta(\%) = \frac{\left|\rho_p\left[\left(\frac{(1-2\eta)U^2}{2(1+\eta)h}+\dot{U}\right)\left(\frac{1-2\eta}{2(1+\eta)}\right)\frac{b^2}{2} - \frac{U^2-\dot{U}h}{3}\right]\right|}{\left|\sqrt{\frac{2}{3}}\lambda\sqrt{1+\frac{1}{2}\left(\frac{1-2\eta}{1+\eta}\right)^2} + \rho_p\left[\left(\frac{(1-2\eta)U^2}{2(1+\eta)h}+\dot{U}\right)\left(\frac{1-2\eta}{2(1+\eta)}\right)\frac{b^2}{2} - \frac{U^2-\dot{U}h}{3}\right]\right|} \times 100$$

IV. Results and discussion

IV.i. Shear frictional energy on consideration of different frictions

Our analysis focused on the contribution of sliding friction (W_f) in three distinct scenarios: sliding without a sticking zone existence, sliding with a sticking zone existence, and only sliding friction. Remarkably, our results revealed that W_f exhibits the highest magnitude when a sticking zone is present, contrasting sharply with the lowest values observed in the case of only sliding friction.

The intermediate scenario of sliding and sticking without a sticking zone was displayed W_f values between these extremes. Furthermore, our findings indicate a notable increase in the difference of W_f with an escalation in the RAM speed(U). Taken $\lambda = 1070.7\text{kg/cm}^2, \mu = 0.3, b = 3.088\text{cm}, h = 1\text{cm}, n = 2.0, \rho_p = 0.0027, \text{kg/cm}^3, \rho = 0.7$ .Notably, after a 15% reduction in height, the discrepancy in W_f became more pronounced. Our study revealed that the die load is maximized when a sticking zone is present, indicating a substantial impact of cohesion on the overall load. In contrast, scenarios involving both sliding and sticking friction without a designated sticking zone exhibited the lowest die load, suggesting that the interplay between these frictional components can lead to a reduction in overall load resistance.

Interestingly, the die load in the case of only sliding friction lies between the two extremes. Furthermore, there is a marked and significant increase in die load after a 15% reduction in height. The die load is greater for preforms with higher relative density compared to those with lower relative density at the same height percentage reduction. After a 20% height reduction, the die load increases very sharply, especially for preforms with a density greater than 0.8.

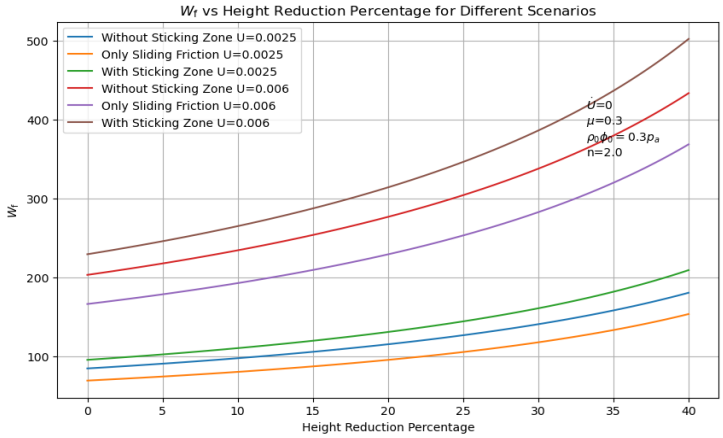

Fig. 1. Variation of frictional energy with height reduction percentage for different frictions at various ram speeds (U).

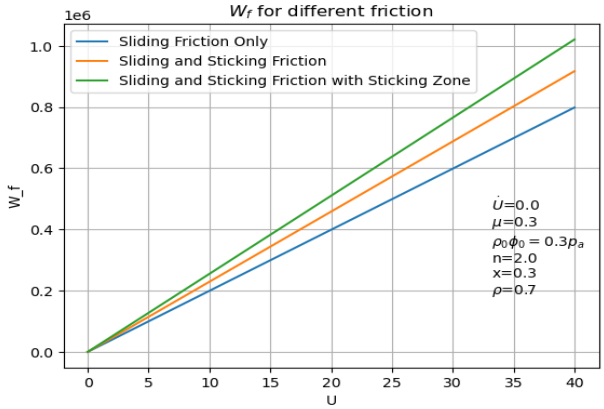

Fig. 2. Variation of frictional energy for different frictions at various ram speeds (U).

By Figure 2, dissipation of shear frictional energy is minimal in the case of only sliding friction, maximal in the case of sliding and sticking friction with a sticking zone, and intermediate in the case of sliding and sticking friction without a sticking zone.

IV.ii. Distribution of friction

Consider only sliding friction in the plastic deformation of a sintered metal powder compact.

$$\tau = \mu \frac{\sqrt{\frac{2}{3}}\lambda\sqrt{1+\frac{1}{2}\left(\frac{1-2\eta}{1+\eta}\right)^2}+\rho_p\left[\left(\frac{(1-2\eta)U^2}{2(1+\eta)h}+\dot{U}\right)\left(\frac{1-2\eta}{2(1+\eta)}\right)\frac{b^2}{2}-\frac{U^2-\dot{U}h}{3}\right]}{1-\frac{2(1-2\eta)\mu b}{(1+\eta)h}\left(\frac{1}{3}\right)}$$

Friction is the same everywhere on the preform surface because it's independent of the term.

Consider sliding friction and sticking friction without a sticking zone.

$$\tau = \mu p_{av}\left[1 + x\left\{1 - \frac{r}{nb}\right\}\right];$$

Friction has a dependency on r.

Consider sliding friction and sticking friction with a sticking zone.

$$\tau = \mu p_{av}\left[1 + x\left\{1 - \left(\frac{r_m - r}{nb}\right)\right\}\right]$$

The coefficient of friction depends on dry friction or lubricated conditions. Friction has a dependency on the distance from the center of preform.

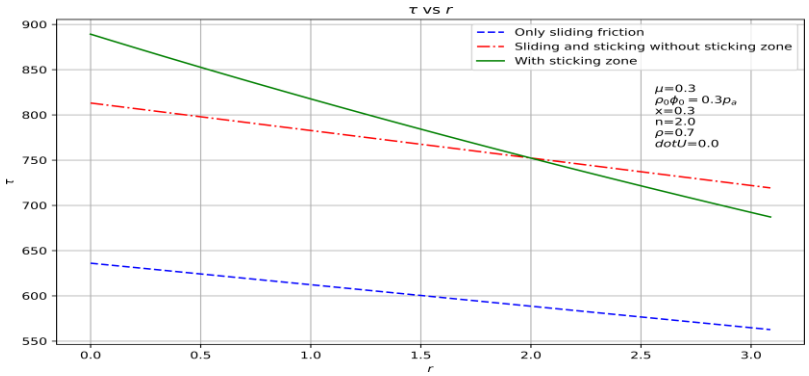

Fig. 3. Comparison of different frictions with radial distance (r).

Figure 3 results indicate that friction is maximized when a sticking zone is present. Sliding friction exhibited the minimum friction, highlighting the dominant role of sliding interactions. Sliding and sticking friction without a sticking zone, friction levels fell between the two extremes, complex interplay between these friction components. Notably, we observed a distinctive radial variation in friction, with a decrease in friction moving outward from the center of the preform. In the presence of a sticking zone, the friction experienced a sharp decline, particularly in comparison to the other two cases. For only sliding, friction exhibited a linear variation with distance from the center. In the case of sliding and sticking friction without a sticking zone, friction initially decreased moderately within the inner half radius of the preform, followed by a rapid decline in the outer half radius.

IV.iii. Impact of Forging Speed

The speed parameter exerts a substantial impact on the forging of sintered preforms, yet there has been relatively limited research conducted on this crucial aspect. The influence of speed on metal preforms during the forging process is a critical factor that can significantly affect various deformation characteristics and final product properties. More in-depth research on the effect of speed will enhance our understanding of its implications in sintered preform forging. Exploring this aspect further could lead to valuable insights for optimizing the forging process, improving

efficiency, and achieving desired material properties in the final products.

$$P = \frac{\sqrt{\frac{2}{3}}\pi\lambda b^2\sqrt{1+\frac{1}{2}\left(\frac{1-2\eta}{1+\eta}\right)^2} + \pi\rho_p b^2\left[\left(\frac{(1-2\eta)U^2}{2(1+\eta)h}+\dot{U}\right)\left(\frac{1-2\eta}{2(1+\eta)}\right)\frac{b^2}{2} - \frac{U^2-\dot{U}h}{3}\right]}{1-\frac{2(1-2\eta)\mu b}{(1+\eta)h}\left(\frac{1}{3}+x\left\{\frac{1}{3}\left(1-\frac{r_m}{nb}\right)+\frac{1}{4n}\right\}\right)}$$

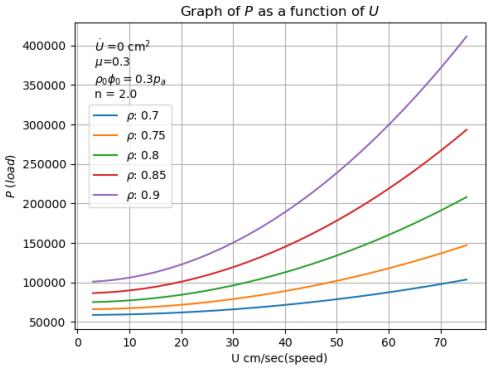

Fig. 4. $\dot{U} = 0\text{cm/sec}^2$

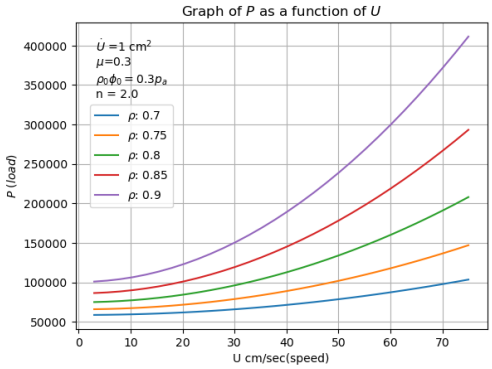

Fig. 5. $\dot{U} = 1\text{cm/sec}^2$

Figure 4, 5: Variation of die load (P) for different initial relative density ρ

Ta $\lambda = 1070.7\text{kg/cm}^2, \mu = 0.3, b = 3.088\text{cm}, h = 1\text{cm}, n = 2.0, \rho_p = 0.0027\text{kg/cm}^3$. For the preforms with higher relative density ρ, a greater load P is needed for deformation. After a velocity of U=10 cm/sec, there is a noticeable spike in the required load P for various relative densities ρ. The rate of change in speed U also influences the increase in required load P.

The internal energy dissipation exhibits a linear relationship with speed, according to the formula of internal energy dissipation. The relationship between internal energy dissipation and speed follows a linear trend, providing a clear and straightforward understanding of how speed changes influence the internal energy dissipation during the metal forming process.

The influence of platen speed becomes pronounced after reaching U = 8 cm/sec, particularly in the inertial energy dissipation across preforms with varying initial relative densities. Interestingly, the rate of change in speed, $\dot{U}$, shows minimal impact on inertial energy dissipation. This observation underscores the significance of platen speed as a key factor influencing inertial energy dissipation, especially beyond the threshold of U = 8 cm/sec.

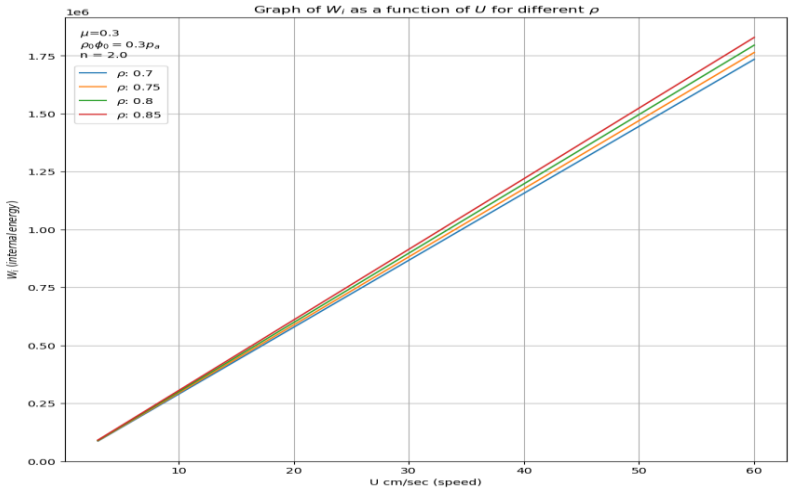

Fig. 6. (a) Variation of W_i with U

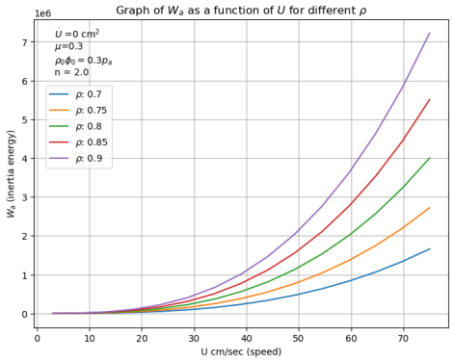

Fig. 7. $\dot{U} = 0$ cm/sec^2

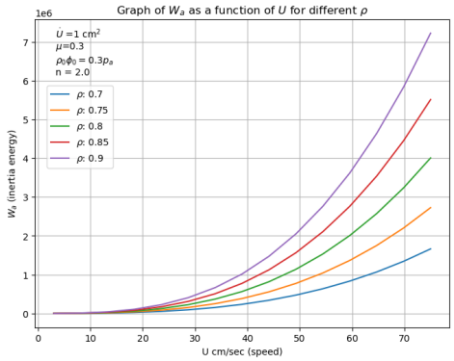

Fig. 8. $\dot{U} = 1$cm/sec^2

Figure 7,8: Variation of W_a with speed U for different ρ

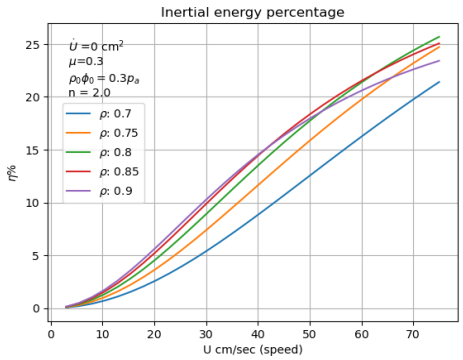

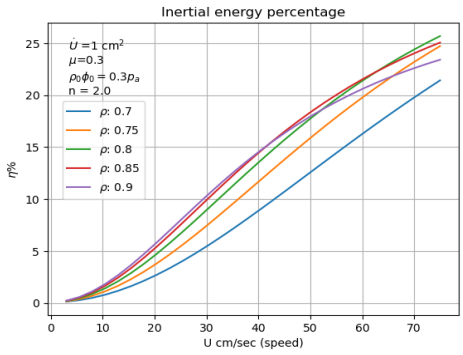

Fig. 9. ($\dot{U} = 0$) & **Fig. 10.** ($\dot{U} = 1$)

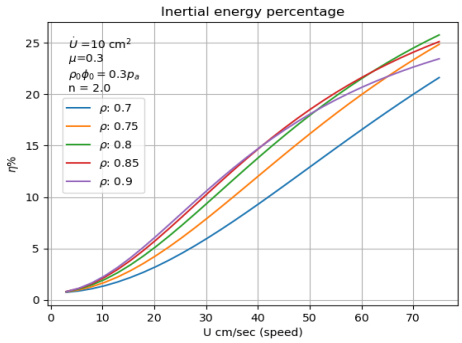

Fig. 11. $\dot{U} = 10$

Figure 9,10,11: Inertial Energy Percentage for different initial relative density ρ

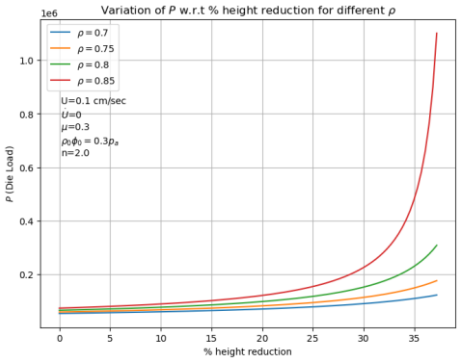

Fig. 12. $U = 0.1$ cm/sec

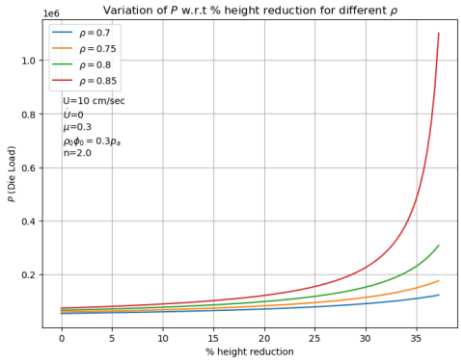

Fig. 14. $U = 10$ cm/sec

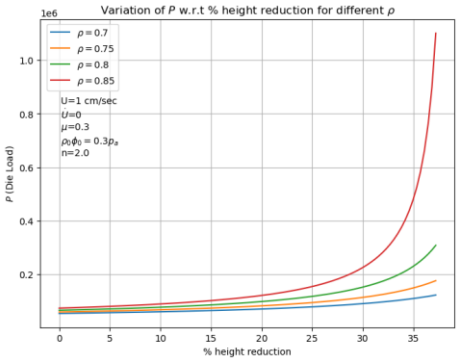

Fig. 13. $U = 1$ cm/sec

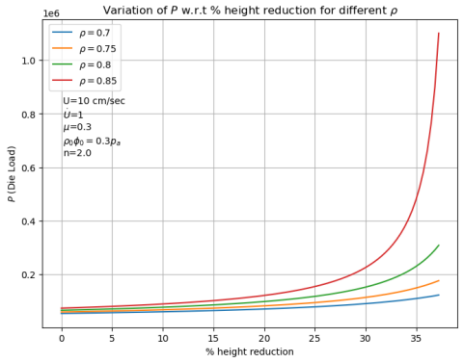

Fig. 15. $U = 10$ cm/sec, $\dot{U} = 1$ cm/sec^2

Figure 12,13,14,15: Variation of P with height reduction percentage for different initial relative density ρ

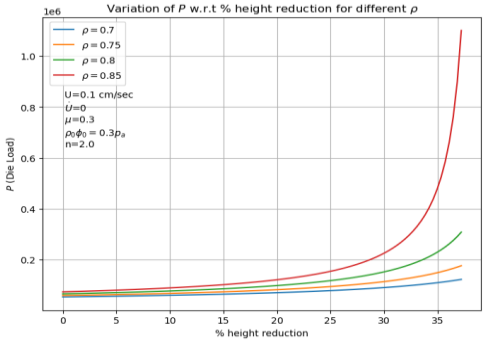

Fig. 16. Variation of load factor for different $\rho = 0.7,0.75,0.8,0.85$

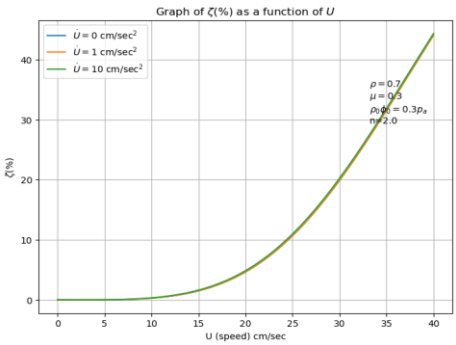

Fig. 17. Variation of load factor with U for different dot U

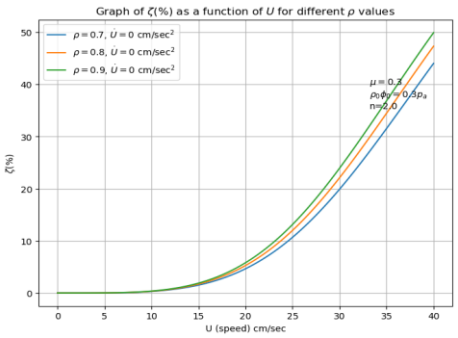

Fig. 19. Variation of load factor for different $\rho = 0.7,0.8,0.9$

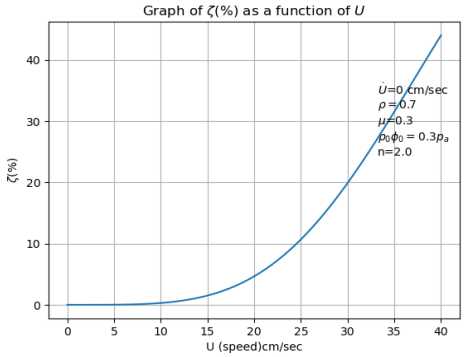

Fig. 18. Variation of load factor with U when $\dot{U} = 0$cm/sec

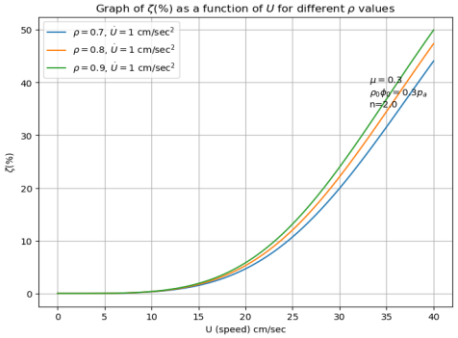

Fig. 20. Variation of load factor for different rho when $\dot{U}$

Fig. 17-20: Variation of $\xi\%$ for different initial relative density in different scenarios.

In our investigation, we observed a consistent trend wherein the inertial factor exhibits lower values for materials with low relative density compared to those with higher relative density. This phenomenon is particularly evident when the relative density is below 0.8 for preforms. The difference in inertial factor becomes more pronounced as the platen speed (U) exceeds 10 cm/sec. Note that beyond a critical speed threshold of 10 cm/sec, the inertial factor experiences a sharp increase. This escalation is particularly significant for materials with a relative density below 0.8.

As the speed changes $\dot{U}$ exceeds, the inertial factor amplifies, especially beyond platen speeds of 10 m/sec. These findings contribute valuable insights to the understanding of inertial factors in materials processing, particularly in scenarios involving varying relative densities and dynamic speed conditions.

Observed that after a 10% reduction in height, there is a noticeable increase in die load P. Subsequently, as the height reduction reaches 15%, the distinction between die loads for various preform relative densities becomes more pronounced. This divergence becomes particularly evident after a 35% reduction in height, where the die load P asymptotically approaches the y-axis. This significant escalation in die load is particularly notable for preforms with high initial relative densities exceeding 0.8. This observation highlights the substantial impact of preform relative density on die load behavior during plastic deformation. There is not much effect of $\dot{U}$ in increasing the die load.

Load factor has a dependency on speed U and initial relative density ρ. Beyond a critical speed threshold of U=10 cm/sec, a sudden increment in the load factor was evident. Further analysis revealed that this difference in load factor became even more apparent after U=15 cm/sec for varying initial relative densities ρ. The load factor exhibited a heightened sensitivity to changes in speed beyond this threshold, with the differences between load factors becoming more pronounced for different ρ values.

Interestingly, the rate of change of speed ($\dot{U}$) showed an amplifying effect on the load factor differences, particularly after U= 15 cm/sec for various initial relative densities ρ. This amplification effect highlights the complex interaction between speed changes and enlightens the need for a comprehensive understanding of these factors.

However, it is noteworthy that for high speeds, the impact of the rate of change of speed ($\dot{U}$) on the load factor appears very clearly. This observation contributes valuable insights into the speed-dependent behavior of the preforms, showcasing the critical speeds at which significant changes in load factor occur and the role of initial relative density in influencing these dynamics. The findings also emphasize the relationship between speed changes and load factor, providing a foundation for further exploration and understanding in performance processing applications.

V. Conclusions

In conclusion, our analysis delved into the dynamics of frictional effects during sintered metal forging, considering different scenarios involving sliding friction, sticking friction, and their combinations. The research explored the variations in die load (P), friction (τ), and the influence of height reduction percentage under different conditions, shedding light on critical aspects of the metal forming process.

The impact of platen speed on the forging of sintered preforms is a critical but relatively underexplored area of research. The speed's influence during the forging process can significantly affect various deformation characteristics and final product properties. An in-depth investigation into the effect of speed can enhance our understanding, offering valuable insights for optimizing the forging process and achieving desired material properties. The required load for deformation increases with

higher relative density (ρ), emphasizing the need for careful consideration of this parameter in the forging process.

• Our findings highlighted the substantial impact of the sticking zone on both die load and friction. Specifically, die load (P) exhibited its highest magnitude in the presence of a sticking zone, while sliding friction (τ) reached its maximum when sticking was involved. In contrast, scenarios with only sliding friction displayed lower die loads and friction values. The intermediate scenario of sliding and sticking without a sticking zone resulted in values between these extremes.

• Moreover, the study underlined the significant role of ram speed (U), showing a notable increase in the difference of die load (W_f) with an escalation in U. The discrepancy in die load became more pronounced after a 15% reduction in height, emphasizing the sensitivity of the process to operational parameters.

• The radial variation of friction revealed distinctive patterns. With the sticking zone, the friction experienced a sharp decline, particularly in the outer half radius of the preform. In contrast, scenarios involving only sliding friction exhibited a linear variation with distance from the center. The case of sliding and sticking friction without a sticking zone showed a moderate decrease within the inner half radius, followed by a rapid decline in the outer half. After a velocity of U = 10 cm/sec, there is a noticeable spike in the required load (P) for various relative densities (ρ). The rate of change in speed ($\dot{U}$) also influences the increase in required load (P). Internal energy dissipation exhibits a linear relationship with speed, providing a clear understanding of how speed changes influence the metal forming process.

• The influence of platen speed becomes pronounced after reaching U= 15 cm/sec, particularly in inertial energy dissipation across preforms with varying initial relative densities. Interestingly, the rate of change in speed ($\dot{U}$) shows minimal impact on inertial energy dissipation, underscoring the significance of platen speed in influencing these dynamics.

• The inertial factor consistently exhibits lower values for materials with low relative density compared to higher relative density. This trend is particularly evident for relative densities below 0.8. Beyond a critical speed threshold of 10 cm/sec, the inertial factor sharply increases, especially for materials with a relative density above 0.8. As the speed changes ($\dot{U}$) exceeds 1 cm/secÂ², the inertial factor amplifies, particularly beyond platen speeds of 10 m/sec.

• After a 10% reduction in height, there is a noticeable increase in die load (P). The distinction between die loads for various preform relative densities becomes more pronounced at a 15% reduction in height. Beyond a 35% reduction, the die load asymptotically approaches the y-axis, especially for preforms with high initial relative densities exceeding 0.8. The impact of $\dot{U}$ on increasing the die load is minimal.

• Load factor dependency on speed (U) and initial relative density (ρ) is evident beyond a critical speed threshold of U = 10 cm/sec, with a sudden increment in the load factor. This difference becomes more apparent after U = 15 cm/sec for varying initial relative densities.

Overall, these insights contribute to a deeper understanding of the complex interplay of frictional forces in sintered metal forging, offering valuable implications for optimizing industrial forging processes and enhancing predictive models in the field.

For high speeds, the impact of $\dot{U}$ on the load factor becomes clearer, emphasizing the critical speeds at which significant changes in load factor occur. These findings contribute valuable insights into the speed-dependent behavior of preforms, offering a foundation for further exploration and understanding in preform processing applications.

Figure 21 illustrates the convergence between the experimental and theoretical curves, particularly noticeable at high height percentage reductions. This observation is consistent with findings reported in reference [4]. The close alignment between experimental and theoretical results underscores the potential applicability of our model within industrial contexts.

This convergence suggests that our model holds promise for accurately estimating die load across diverse operational parameters, including speed variations, initial relative density discrepancies, alterations in preform dimensions, and variations in the degree of adhesion during height reduction processes. The implications of our model for industrial processes are significant, as it offers the capability to precisely estimate die load under varying conditions. Such predictive capabilities are crucial for optimizing manufacturing processes, enhancing efficiency, and ensuring product quality.

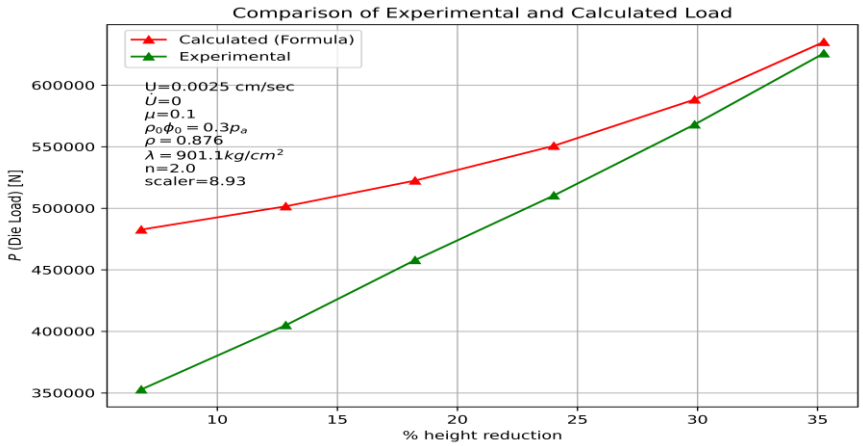

Fig. 21. Validation

VI. Acknowledgments

Navdeep's work is supported by the Council of Scientific and Industrial Research (CSIR), Govt. of India (Award no. 09/1256(15849)/2022-EMR-1). Dr. Parveen Kumar expresses his gratitude for the financial support from the Department of Science & Technology, New Delhi, India, for the Purse (SR/PURSE/2022/126).

Appendics

[A] Velocity field, Strain rates

$$U_r = \frac{(1-2\eta)}{2(1+\eta)}\frac{U}{h}r, U_z = -z\frac{U}{h}, U_\theta = 0 \text{ satisfy } \frac{\partial U_r}{\partial r} + \frac{(1-2\eta)}{2(1+\eta)}\frac{\partial U_z}{\partial z} = 0$$

Choose the kinetically admissible velocity field which satisfies the boundary condition,$|U_z|_{z=0} = 0$ and $|U_z|_{z=h} = U$.

Strain rates $\dot{\varepsilon}_{rr} = \frac{\partial U_r}{\partial r} = \frac{(1-2\eta)}{2(1+\eta)}\frac{U}{h}$; $\dot{\varepsilon}_{\theta\theta} = \frac{U_r}{r} = \frac{(1-2\eta)}{2(1+\eta)}\frac{U}{h}$; $\dot{\varepsilon}_{zz} = \frac{\partial U_z}{\partial z} = -\frac{U}{h}$; $\dot{\varepsilon}_{rr} = \dot{\varepsilon}_{\theta\theta}$

$\dot{\varepsilon}_{r\theta} = \frac{1}{2}\left(\frac{\partial U_\theta}{\partial r} - \frac{\partial U_\theta}{\partial r} + \frac{1}{r}\frac{\partial U_r}{\partial \theta}\right) = 0$; $\dot{\varepsilon}_{rz} = \frac{1}{2}\left(\frac{\partial U_r}{\partial z} + \frac{\partial U_z}{\partial r}\right) = 0$; $\dot{\varepsilon}_{\theta z} = \frac{1}{2}\left(\frac{\partial U_z}{\partial \theta} + \frac{\partial U_\theta}{\partial z}\right) = 0$

[B] Upper bound limit analysis

$\boldsymbol{\eta = 0.54(1-\rho)^2}$; $\boldsymbol{\lambda = \frac{\rho^n \sigma_o}{(1-2\eta)}}$; $\boldsymbol{J^* = W_i + W_f + W_a = PU}$

$$J^* = \frac{2\sigma_0}{\sqrt{3}}\int_v \sqrt{\frac{1}{2}\dot{\varepsilon}_{ij}\dot{\varepsilon}_{ij}}\,\mathrm{d}v + \int_s \tau|\Delta V|\mathrm{d}s + \int_v \rho_\mathrm{p} a_i U_i\,\mathrm{d}v$$

$W_i = \frac{2\sigma_0}{\sqrt{3}}\int_v \sqrt{\frac{1}{2}\dot{\varepsilon}_{ij}\dot{\varepsilon}_{ij}}\,\mathrm{d}v$; $W_f = \int_s \tau|\Delta v|\mathrm{d}s$; $W_f = \int_0^b \tau(|U_r|_{z=0} + |U_r|_{z=h}).2\pi r dr$

$W_a = \int_v \rho_\mathrm{p} a_i U_i\,\mathrm{d}v$where $a_r = U_r\frac{\partial U_r}{\partial r} + U_z\frac{\partial U_r}{\partial z} + \frac{\partial U_r}{\partial t}$ $a_z = U_z\frac{\partial U_z}{\partial z} + \frac{\partial U_z}{\partial t}$

[C] Interfacial Friction

Friction has a vital role in metal forming[15], influencing the shaping of the metal workpiece. Sliding friction $\tau = \mu p$, sliding friction and sticking friction without a sticking zone $\tau = \mu\left[p + \rho_0\phi_0\left\{1 - \frac{r}{nb}\right\}\right]$, sliding friction and sticking friction with sticking zone$\tau = \mu\left[p + \rho_0\phi_0\left\{1 - \left(\frac{r_\mathrm{m}-r}{nb}\right)\right\}\right]$in the plastic deformation of a sintered metal powder compact. The sticking radius [18] increases with the height reduction of the metal preform, while sliding friction operates on the remaining portion. Understanding and accounting for both sliding friction and adhesion are crucial for a comprehensive analysis of the metal forming process.

$$r_m = b - \frac{h}{2\mu}\cdot\log\left(\frac{1}{\sqrt{3}\mu}\right)$$

Rooks' Law is a refinement of Coulomb friction. It shows the dependency of the friction coefficient changes with slip velocity and the evolving state of the sliding interface.

Nomenclature

h instantaneous thickness of the workpiece
n constant quantity much greater than unity
p pressure at the die-workpiece interface
P die load and r, θ, z cylindrical co-ordinates
U die velocity, $\dot{U}$ acceleration and U_i displacement rate field
ΔV magnitude of the relative velocity

b radius of the disc and x, y, z Cartesian co-ordinates

ε strain and $\dot{\varepsilon}_{ij}$ corresponding strain rate tensor field

η constant and a function of relative density ρ

λ flow stress of the sintered material and μ coefficient of friction

ρ_{p} initial density of the sintered preform and a_i associated acceleration field

σ_0 yield stress of the non-workhardening matrix metal

τ shear stress and ϕ_0 specific cohesion of the contact surface

W_i internal energy dissipation, W_f frictional shear energy and W_a intertia force energy

$$\xi(\%) = \left(|p/\lambda|_{\text{withdynamiceffect}} - |p/\lambda|_{\text{withoutdynamiceffect}}\right)/|p/\lambda|_{\text{withdynamiceffect}}$$

Conflict of interest

The author declare no conflicts of interest in this paper.

References

I. Agrawal M., Jha A. K., Kumar S., "High-speed forging of hollow metal powder preforms", Inst. Engrs. (I) J., 80 (1999),8.

II. Avitzur B., "Metal Forming Processes and Analysis", McGraw Hill, New York, 1968.

III. Cost savings win the day for PM parts, Metal Powder Report, Vol. 56, Issue 7-8, (2001), 10-14.

IV. Jain Shrikant, Ranjan R. K. and Kumar Surender, "Fracturing and Deformation Characteristics of Aluminium Preform during Cold Forging at Low Strain Rates". Int. J. of Scientific Engineering and Technology, 4(3) (2015),182-186. 10.17950/ijset/v4s3/314

V. Jha A. K and Kumar S., "Analysis of Axisymmetric Cold Processing of Metal Powder Preforms", Journal of the Institution of Engineers (India), 65, (1985), 169.

VI. Jha A. K. and Kumar S., "Compatibility of sintered materials during cold forging", International Journal of Materials and Product Technology, Vol. 9, Issue 4-6, (1994), 281-299. 10.1504/IJMPT.1994.036423

VII. Jha A. K., Kumar S., "Dynamic effects during a high-speed sinter-forging process", International Journal of Machine Tools and Manufacture, Vol. 36, Issue 10, (1996), 1109-1122, ISSN 0890-6955. 10.1016/0890-6955(95)00122-0

VIII. Jha A. K., Kumar S., "Compatibility of sintered materials during cold forging", International Journal of Materials and Product Technology' 9, Issue 4-6, (2004), 281-299. 10.1504/IJMPT.1994.036423

IX. Jones P. K., "The technical and economic advantage of powder forged products", Powder Metallurgy, Vol. 13, Issue 26, (1970), 114-129.

X. Kumar Parveen, Ranjan R. K., Kumar Rajive, **"**Mechanics of deformation during open die forging of sintered preform: Comparative study by equilibrium and upper bound methods", ARPN Journal of Engineering and Applied Sciences, 6(6), (2011)83–93. https://arpnjournals.com/jeas/research_papers/rp_2011/jeas_0611_515.pdf

XI. Kumar Parveen, Ranjan R. K., Kumar Rajive, "Investigations of an axisymmetric compound flow behavior of sintered preform: An upper bound approach", International Journal of Pure and Applied Mathematics, Vol. 81, Issue 5, (2012), 671-691. https://www.ijpam.eu/contents/2012-81-5/2/2.pdf

XII. Kumar Parveen, Ranjan R. K., Kumar Rajive, "Mathematical modelling of forging of sintered preform: Comparative study of open and closed die", International Journal of Pure and Applied Mathematics, Vol. 82, Issue 2, (2012), 179-188. https://www.ijpam.eu/contents/2013-82-2/2/2.pdf

XIII. Kumar Parveen, Ranjan R. K., "Investigation on sintered preform with different geometrical shape", AIP conference Proceedings, Volume 2142, 2019. 10.1063/1.5122620

XIV. Ranjan R. K. and Kumar S., "Effect of interfacial friction during forging of solid powder discs of large slenderness ratio". Sadhana, 29, 535-543, 2004. 10.1007/BF02703260

XV. Rooks B. W., "The effect of die temperature on metal flow and die wear during high-speed hot forging", In Proceedings of the Fifteenth International Machine Tool Design and Research Conference, Springer, (1975), 487-494

XVI. Singh S., Jha A. K., "Sintered preforms adds better value to aerospace components", Journal of Aerospace Engineering, I. E. (I), 82, (2001), 1-6.

XVII. Singh Saranjit, Jha A.K., "Analysis of dynamic effects during high-speed forging of sintered preforms", Journal of Materials Processing Technology, Volume 112, Issue 1, 2001,Pages 53-62, ISSN 0924-0136 10.1016/S0924-0136(00)00898-0

XVIII. Singh S., Jha A. K., "An energy analysis during forging of sintered truncated conical preform at high-speed", Tamkang J. of Science and Engineering,7,(2004),227-236. http://jase.tku.edu.tw/articles/jase-200412-7-4-05

XIX. Singh Saranjit & Jha A. K. & Kumar Suhas. "Dynamic effects during sinter forging of axi-symmetric hollow disc preforms", International Journal of Machine Tools and Manufacture, Vol. 47, Issue 7-8,(2007),1101-1113. 10.1016/J.IJMACHTOOLS.2006.09.023

XX. Tabata T., Masaki S. and Abe Y.,"Analysis of Forging P/M Preforms" Journal of the Japan Society for Technology of Plasticity, 18, (1977), 373.

XXI. Tabata T., Masaki S. and Hosokawa K., "A Compression Test to Determine the Coefficient of Friction in Forging P/M Preforms", International Journal of Powder Metallurgy Powder Technology, 16, (1980), 149.